Comparison Of Mapping And Track Fitting Procedures For FE-I4 500x25μm Sensors.

Ryan Nelson

c/o Dr. Kenneth Gibb Wraight, Dr Alexander Morton, Department of Physics & Astronomy, University of Glasgow.

1106793n@student.gla.ac.uk

Abstract. As the 2023 Atlas Pixel Detector upgrade draws closer research is necessary into new geometries and materials for detector chips that will produce increased performance and boost radiation hardiness. The FE-I4 is the latest front end chip and is planned to be utilised in the upgrade. Through looking at the case of 500x25μm geometry it has been determined how to appropriately map raw data from the default 250x50μm readout to correspond to the 500x25μm pixel geometry. Furthermore through the use of EUTelescope software, three datasets using the 500x25μm detectors have been analysed from DESY and SLAC. Using two different fitting methods, DAFFitter and General Broken Lines (GBL), it has been established the GBL procedure shows a marked improvement on the detector residuals over DAFFitter and that this is consistent over more than one data set. This is an important result that implies GBL is a better fitting procedure and will allow research in the future to have confidence in it when analysing other detector geometries and types outside the scope of this investigation.

1. Introduction

1.1. Atlas and the Pixel Detector

The Atlas detector at CERN is a large multipurpose detector consisting of a series of detector systems that are cylindrically concentric about the interaction point. One such system is the inner tracker, itself comprised of cylindrical barrel sections responsible for tracking charged particles by measuring there interaction with material, yielding information on particle type, charge and momentum. The inner most section is known as the Pixel Detector, here there are 1744 modules with 47000 pixels per module giving extremely accurate tracking near the interaction point [5]. As they are so close to the interaction a primary challenge is ensuring the pixel detectors are radiation hardened, which allows them to operate optimally even after significant exposure. It is therefore planed for an inner tracker upgrade during Long Shutdown 3 due to take place ~2023 where by detectors will be replaced for improved resolution, readout rate, and radiation hardiness [5].

1.2. Detector chips

Research and development aims at investigating different chip materials, geometries and different irradiated states. Detectors operate by radiation producing ions in the detector material with a biasing voltage pulling that charge down to the readout channels where the charge collection forms an electronic signal. Each chip consists of an array of readout channels bump-bonded to a large sensitive bulk, usually made of silicon. This arrangement forms a series of discrete sensitive elements known as pixels. Charge has a tendency to diffuse across multiple pixels over time. This is why the role of biasing is of great importance, an electric field pulls the charge down quickly which prevents the

dispersion. It requires a minimum bias to permeate across the whole bulk for a given thickness. Any less than this and the bulk is known to be under depleted, and similarly over depleted if the bias is of a greater value [5]. Sub-pixel resolution can be determined from analog readout which allows a determination of charge weighting between clusters of pixels. Additionally noise may be responsible for producing a low background signal due to free charge carriers at the operating temperature. A threshold value is introduced which is a minimum required signal, charge readout is measured as time over threshold (ToT) and to ensure all readout channels are homogenous they are tuned by a standardised pulse, ie. Set to readout the same value [5].

1.3. The FEI4

The Atlas upgrade will make use of new Front End chips of which FEI4 is the latest version. It has 80 columns and 336 rows giving 26880 readout channels with a pixel pitch of 250x50μm for standard geometry. Alternative geometries are available including pixel pitches of 500x25μm forming 40 columns and 672 rows and will be the subject of this investigation [1].

The FEI4 chips are examined in the test beam environment where monochromatic high energy particles are fired at the detector in order to gauge its response. Test beam facilities in operation include DESY in Hamburg (4-5GeV electrons) and SLAC in Stanford (12.5GeV electrons) [5] from which several datasets will be studied in this investigation. To measure the particle trajectories before and after the detectors (known as DUTs) a series of well known detectors are arranged before and after the DUT, usually mimosa 26s, which allow interpolation of the interaction point on the DUT. This expected position can be compared with the measured position on the device and the difference between these points is known as the residual.

Information is obtained through hits on each plane. Each activated pixel has a local x and y coordinate on the pixel array and charge is deposited in ToT. These local parameters need to be transformed into a common global geometry from which tracks can be reconstructed using information from the hits and comparisons with the DUT made. It also requires many tracks to be reconstructed to have a sufficient statistical accuracy.

1.4. EUTelescope

The analysis of this data is performed by the EUTelescope software. It consists of a series of steps using the LCIO data format to take the raw data and finally calculate a resolution for the detector under inspection, with in depth ROOT output for each step along the way. The first step is the converter step from which the raw data is converted using eudaq to LCIO format [2][3]. Hot pixels that are temperamental and lead to false hit readings are also marked at this stage. User input can define a cut-off frequency for which any pixel firing more frequently than this defined parameter are determined to be hot pixels which will later be discarded.
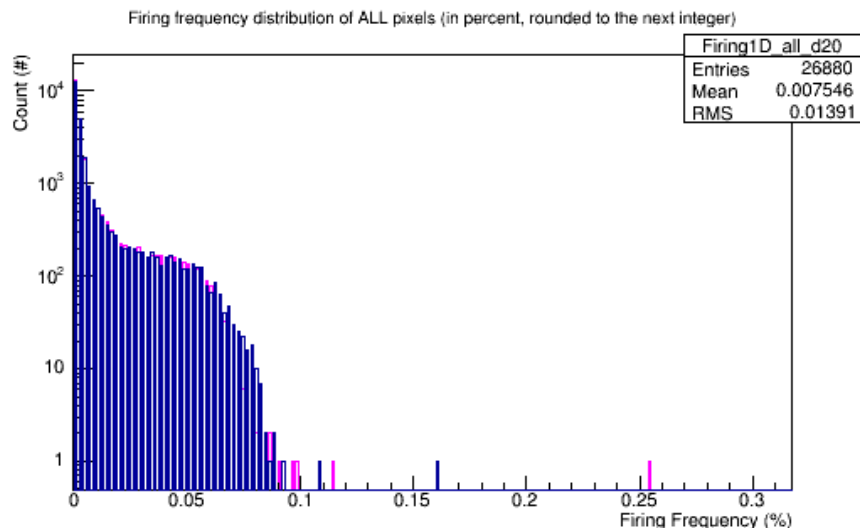

Figure 1: Overlay of firing frequency of all pixels for both DUTs

(Approximately 0.1 here would be a good cut off frequency)

Following this for irregular geometries a mapping step is introduced where the readout channel data is rearranged to correspond to the physical position of the activated pixel. Failing to do this can result in senseless clustering as adjacent readout channels may not correspond to adjacent pixels [1]. Next is the clustering step which looks at the eight nearest neighbours of an activated pixel to see if they too are activated, if so these pixels are grouped as a cluster and iteratively the eight nearest neighbours of those pixels are looked at and so on to potentially expand the size of the cluster. Any cluster that contains an identified hot pixel is also discarded at this point [3]. The following steps are hitmaker, which globally orientates the planes and facilitates checking that each plane is correctly correlated with respect to one and other. An anti correlation would imply the considered planes are in some regard rotated/flipped with respect to one another.
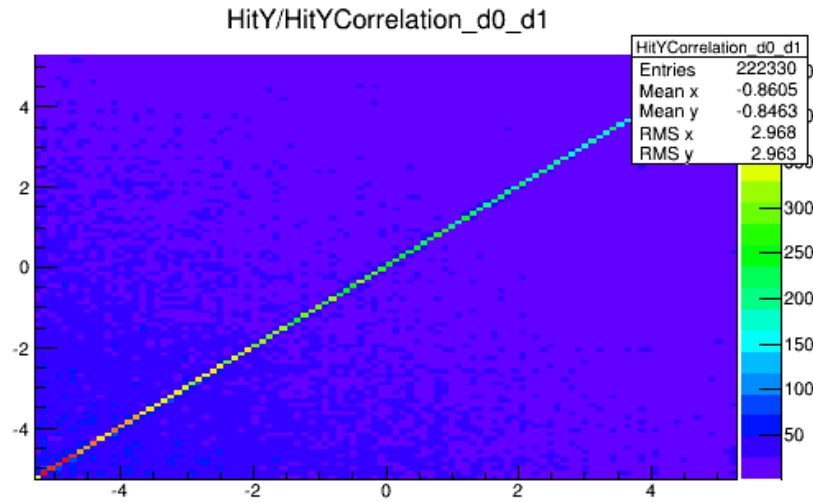

Figure 2: Postive correlation. Implies planes are correctly aligned in this case in the Y dimension.

Following hitmaker are the align and fitter steps which use pattern recognition and track fitting to globally align the planes then generates tracks which can be used to calculate the DUT resolution. In this study we will look at two methods of alignment and fitting, General Broken Lines (GBL) and DAFFitter. All track fitters use a least squares approach, DAFFitter and GBL attempt to minimise the chi square distribution of each of their hit residuals in order to fit a track. This can only be done where the Gauss Markov theorem assumptions hold true [4]. These assumptions are defined as:

- The measurements must be unbiased.
- All normalized residuals necessarily have identical variance.
- The measurement errors must be uncorrelated between planes.

For these to be true the geometry must be correctly described with numerical techniques, the covariance matrix of residuals must correctly describe the residual error and it must be ensured that systematic measurement errors do not result in correlations between planes. The EUTelescope procedure ensures these conditions are met.

1.5. DAFFitter
    DAFFitter performs pattern recognition through grouping together each plane as if they all lay on a single plane and associates hits together if they fall within a specified radius of a hit on the first plane. Track fitting operates under the assumption that pattern recognition is not perfect and they are fitted through down weighting outlying hits through raising the resolution of the appropriate plane. Milipede then performs the alignment procedure by seeking to minimise the residuals and hence the chi squared for all hits on each plane[2].

1.6. General Broken Lines
    The GBL procedure performs pattern recognition by forming triplets (groups of 3 hits, one on each plane) on both the upstream and downstream arms of the telescope. To assess if certain hits form a triplet there is a series of cuts that first act to form a doublet with hits on the first and third plane on each arm, then another cut to form a triplet which looks for an associated hit on the second plane of each arm. These triplets meet in the middle of the telescope and a further cut deduces if both triplets coincide to form a track [2]. Once two triplets are identified as forming a track, each hit is parameterised as a straight line. The track is then extrapolated or interpolated to form a predicted hit on a DUT.

    Alignment generates matrices that determine the offsets of each point in the global frame when each plane is shifted. Of course each hit position is fixed locally but movement of the plane it lies on results in a global coordinate change. Track intersection points on the DUTs are also shifted by the corrections and are extrapolated with the same incidence to the DUT plane giving a corrected interaction point on the plane [2].

    Matters are further complicated through scattering. There are two types of scatterer, thick and thin. In thin scattering the entire radiation length, the length over which incoming radiation loses 1/e of its energy, is located at one point. In the track frame of reference thin scattering is accounted for as a propagating cone which is representative of the error introduced by the scattering. Of course how this cone interacts with subsequent planes is not trivial and the cone must be converted from the track frame to the local frame of the detector, non-diagonal terms are introduced in the covariance matrix and the cone becomes an ellipse in the local frame [2].

    Thick scatterers have a non negligible radiation length and hence there will be a change in position from the start of the material to the end. These can be approximated by two thin scatterers for any inhomogeneous material, the positions of these thin scattering points depends on the distribution of the material. These inhomogeneous materials are represented within EUTelescope as blocks of homogeneous material which simplifies the problem of integrating along the tracks path to simply adding these blocks together.

    Scattering results in broken lines and so the tracks are fitted by again minimising the chi-squared distribution given the limitations placed on the arrangement by the scattering.

2. Method
This study focuses on three sets of test beam data, two runs from DESY, November 2013 and February 2014 and an additional run from SLAC in May 2014. Each arrangement comprises of two 500x25 FE-I4 DUTs and six mimosa planes, each with differing z positions and states of irradiation.

    Analysis of each set is performed by EUTelescope, the geometries of the DUTs and positions of the planes are initialized in an individual gear file for each run. As these sets involve the non-standard 500x25 geometry, the output must be mapped to ensure hit positions are correctly represented and proper clusters are formed.

    For the 500x25 geometry two versions of mapping are potentially applicable.

```
if(nCol==40 && nRow==672)
    if(col%2==1){
        geoRow=row*2/1 +1;
        geoCol=(col)*1/2;
    }
    else{
        geoRow=row*2/1;
        geoCol=(col-1)*1/2;
    }
}
```

Mapping version 1.

```
if(nCol==-40 && nRow==672){
    if(col%2==1){
        geoRow=row*2/1 ;
        geoCol=(col-1)*1/2;
    }
    else{
        geoRow=row*2/1 +1;
        geoCol=(col)*1/2;
    }
}
```

Mapping version 2.

Using Data from run 692 of DESY November 2013 and run 186 of DESY February 2014. Clustering is run for both datasets using both mapping versions individually. An additional comparison is made by also running both mapping versions with the geometric clustering technique as opposed to sparse clustering to identify any differences between the two methods.

One would expect the average cluster size in X to decrease with an appropriately mapped version as the 500μm x pixel pitch would require a large amount of charge dispersion to form clusters of a greater size than one in this dimension. Similarly the smaller 25μm y pitch should lead to increased average cluster size in this dimension. It is also expected for the multiplicity to behave in a reciprocal manner to the average signal as more events leads to charge dispersed among more clusters.

In the converter step hot pixels are designated by examining the total firing frequency log graphs for both DUTs and asserting a cut off value that corresponds to the visibly anomalous firing pixels (figure 2).

Having ascertained the correct mapping version, EUtelescope is followed through the hitmaker, alignment and fitter steps, initially using DAFFitter which allows after sufficiently tightening the cuts production of the x and y residuals for the two DUTs in each arrangement.

A repeat process takes place after the DAFFitter analysis but using the GBL fitting procedure instead. The EUTelescope source code was modified to include histograms that return the separation distance of all doublets and triplets considered which allows us to place confidently accurate cuts when forming tracks. Upon completion this allows a comparison between the residuals produced by DAFFitter with those produced by GBL from which it can be inferred which one is a more accurate track fitting procedure. A second level of comparison is the results of this between multiple datasets, are the results consistent across different test beams which will have unique geometrical arrangements.

3. Results

3.1. DESY November 2013 Mapping comparison.

Mapping Version	Signal (± RMS)	Cluster Size X (± RMS)	Cluster Size Y (± RMS)	Multiplicity (± RMS)
Version 1 Detector 20 (Clustering)	9.591 ± 4.315	1.031 ± 0.1755	1.643 ± 0.8859	1.132 ± 0.4904
Version 1 Detector 21 (Clustering)	7.833 ± 3.703	1.024 ± 0.1551	1.755 ± 0.8882	1.123 ± 0.4796
Version 2 Detector 20 (Clustering)	7.532 ± 3.968	1.027 ± 0.163	1.29 ± 0.6884	1.442 ± 0.7923
Version 2 Detector 21 (Clustering)	6.263 ± 3.453	1.021 ± 0.1451	1.403 ± 0.7319	1.404 ± 0.7787
No Mapping Detector 20 (Clustering)	9.639 ± 4.527	1.529 ± 0.5613	1.346 ± 0.6337	1.126 ± 0.4446
No Mapping Detector 21 (Clustering)	7.834 ± 3.855	1.614 ± 0.5449	1.312 ± 0.5949	1.123 ± 0.4546

Device/Mapping Version	Signal (± RMS)	Cluster Size X (± RMS)	Cluster Size Y (± RMS)	Multiplicity (± RMS)
Version 1 Detector 20 (GeoClustering)	9.591 ± 4.315	1.031 ± 0.1755	1.643 ± 0.8859	1.132 ± 0.491
Version 1 Detector 21 (GeoClustering)	7.833 ± 3.703	1.024 ± 0.1551	1.755 ± 0.8882	1.123 ± 0.4801
Version 2 Detector 20 (GeoClustering)	7.532 ± 3.968	1.027 ± 0.163	1.29 ± 0.6884	1.442 ± 0.795
Version 2 Detector 21 (GeoClustering)	6.263 ± 3.453	1.021 ± 0.1451	1.403 ± 0.7319	1.404 ± 0.7799
No Mapping Detector 20 (GeoClustering)	9.639 ± 4.527	1.529 ± 0.5613	1.346 ± 0.6337	1.126 ± 0.4451
No Mapping Detector 21 (GeoClustering)	7.834 ± 3.855	1.614 ± 0.5449	1.312 ± 0.5949	1.123 ± 0.4546

Figure 3:

3.2. DESY February 2014 mapping comparison.

Device/Mapping Version		Signal (± RMS)	Cluster Size X (± RMS)	Cluster Size Y (± RMS)	Multiplicity (± RMS)
Version 1 Detector 20 (Clustering)		6.05 ± 3.55	1.009 ± 0.09599	1.149 ± 0.393	0.4589 ± 0.6033
Version 1 Detector 21 (Clustering)		4.702 ± 2.269	1.005 ± 0.07177	1.1 ± 0.3539	1.053 ± 0.3105
Version 2 Detector 20 (Clustering)		5.787 ± 3.329	1.008 ± 0.09062	1.099 ± 0.3219	0.4797 ± 0.6444
Version 2 Detector 21 (Clustering)		4.518 ± 1.995	1.005 ± 0.07082	1.057 ± 0.2624	1.096 ± 0.3952
No Mapping Detector 20 (Clustering)		6.222 ± 3.649	1.146 ± 0.3617	1.091 ± 0.3248	0.4462 ± 0.565
No Mapping Detector 21 (Clustering)		4.74 ± 2.358	1.09 ± 0.2982	1.059 ± 0.2596	1.045 ± 0.2869
Version 1 Detector 20 (GeoClustering)		6.05 ± 3.55	1.009 ± 0.09599	1.149 ± 0.393	0.4589 ± 0.6033
Version 1 Detector 21 (GeoClustering)		4.702 ± 2.269	1.005 ± 0.07177	1.1 ± 0.3539	1.053 ± 0.3105
Version 2 Detector 20 (GeoClustering)		5.787 ± 3.329	1.008 ± 0.09062	1.099 ± 0.3219	0.4797 ± 0.6444
Version 2 Detector 21 (GeoClustering)		4.518 ± 1.995	1.005 ± 0.07082	1.057 ± 0.2624	1.096 ± 0.3952
No Mapping Detector 20 (GeoClustering)		6.222 ± 3.649	1.146 ± 0.3617	1.091 ± 0.3248	0.4462 ± 0.565
No Mapping Detector 21 (GeoClustering)	4.74 ± 2.358	1.09 ± 0.2982	1.059 ± 0.2596	1.045 ± 0.2869	

Figure 4:

3.3. DESY November 2013 DAFFitter X residuals.
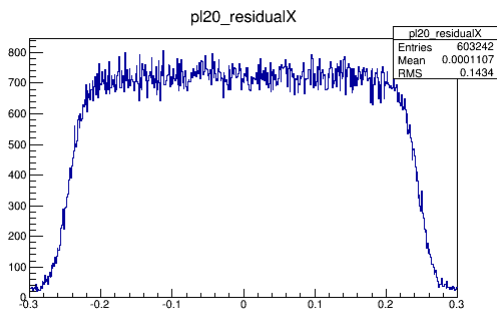
Figure 5:
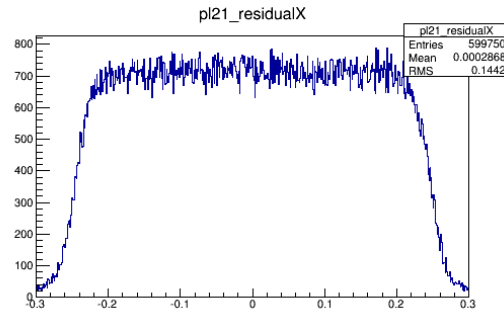
Figure 6:

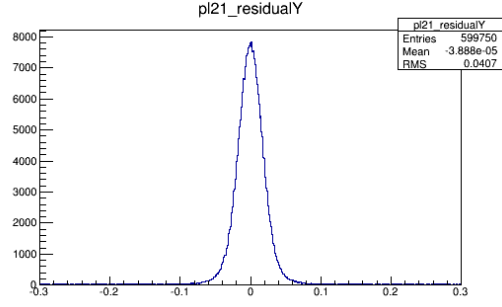## 3.4. DESY November 2013 DAFFitter Y residuals.
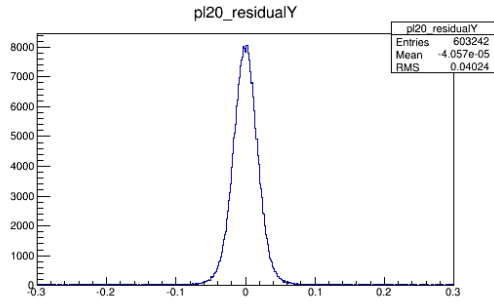
Figure 7:

Figure 8:

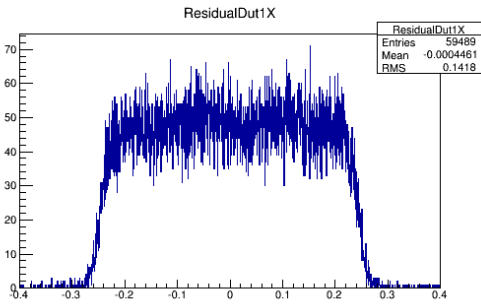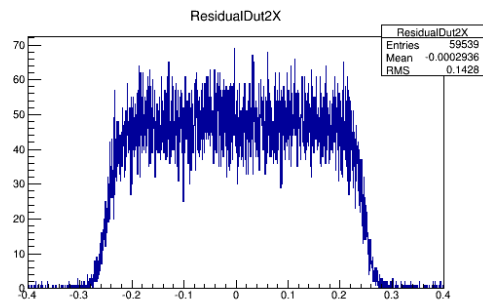### 3.5. DESY November 2013 GBL X residuals.

Figure 9:

Figure 10:
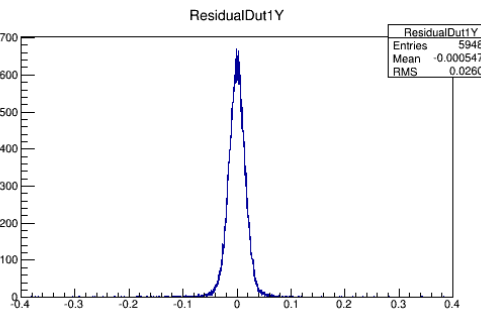
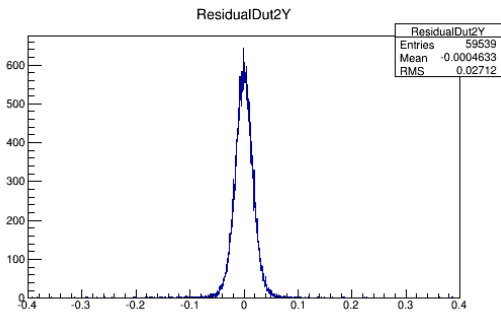### 3.6. DESY November 2013 GBL Y residuals.

Figure 11:

Figure 12:
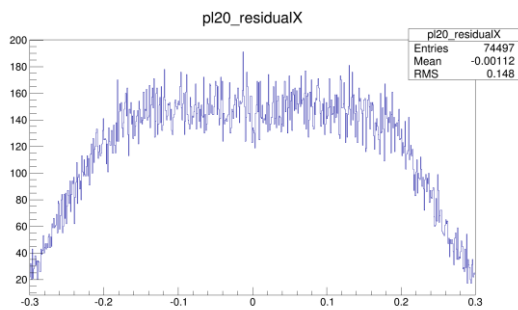
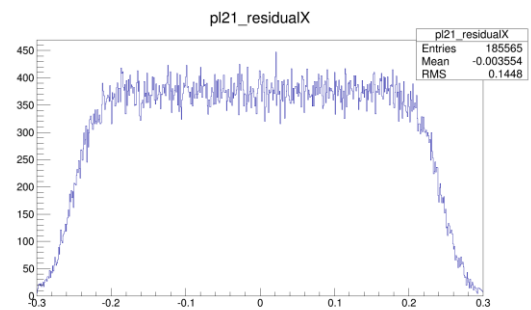### 3.7. DESY February 2014 DAFFitter X residuals.

Figure 13:

Figure 14:

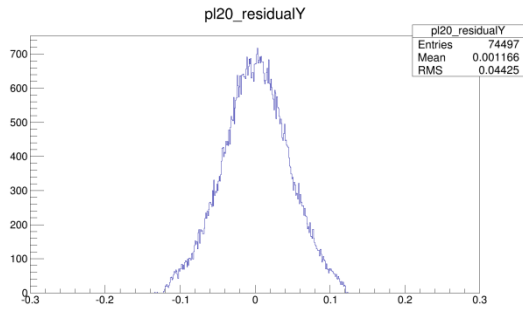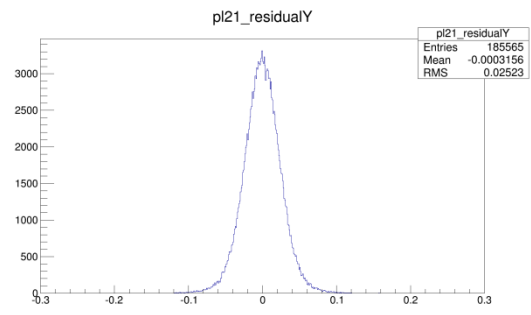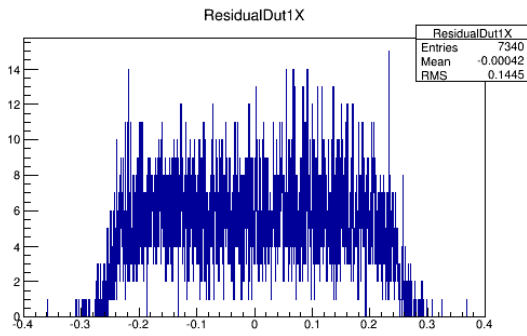### 3.8. DESY February 2014 DAFFitter Y residuals.

Figure 15:

Figure 16:

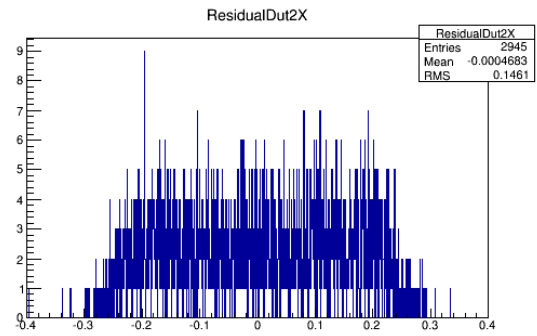### 3.9. DESY February 2014 GBL X residuals.

Figure 17:

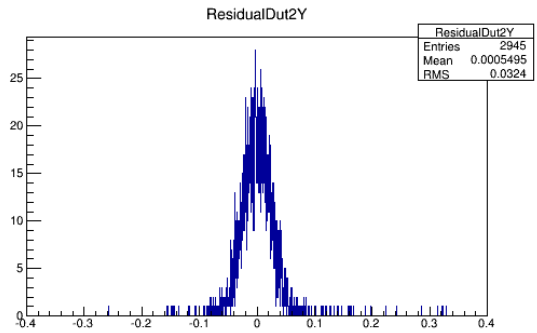

Figure 18:

3.10. DESY February 2014 GBL Y residuals.
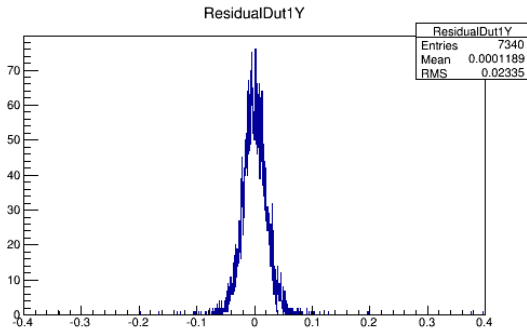
Figure 19:

Figure 20:

3.11. SLAC May 2014 DAFFitter X residuals.
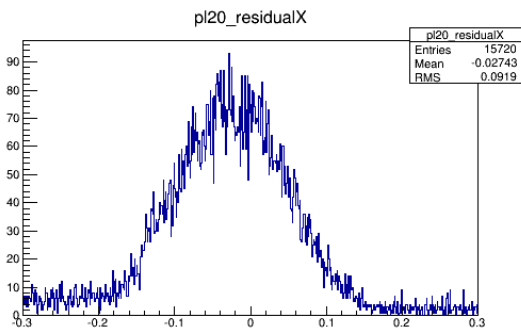
Figure 21:
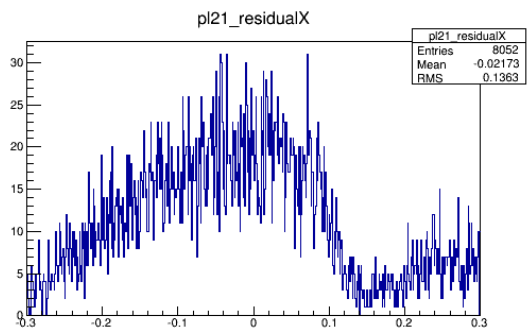
Figure 22:

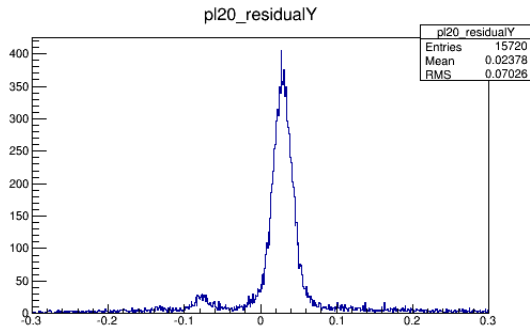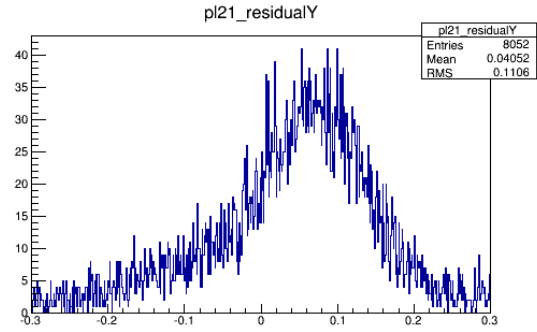### 3.12. SLAC May 2014 DAFFitter Y residuals.

Figure 23:

Figure 24:
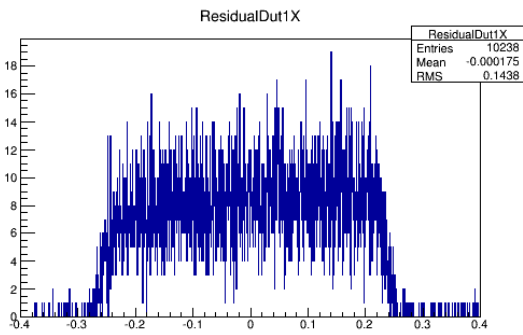
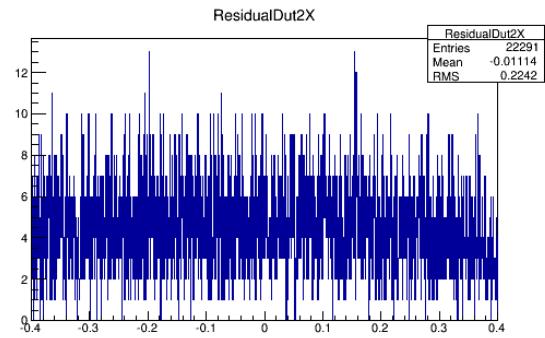### 3.13. SLAC May 2014 GBL X residuals.

Figure 25:

Figure 26:
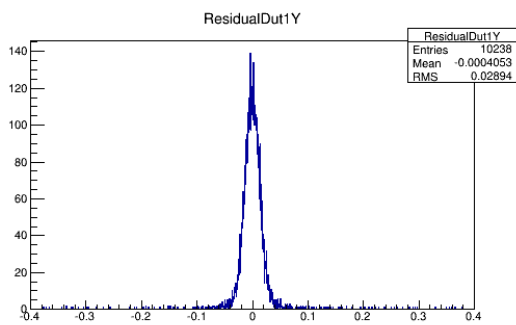
3.14. SLAC May 2014 GBL Y residuals.
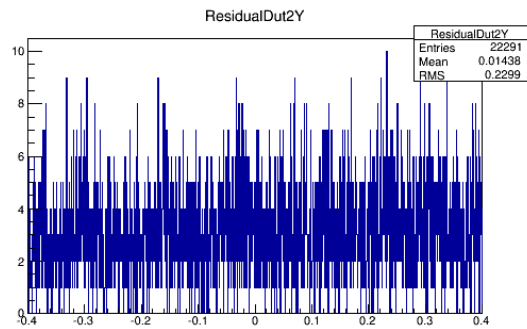

Figure 27:

Figure 28:

4. Conclusion

From the clustering parameters obtained from examining the two sets of DESY data is evident mapping version 1for the 500x25μm appears to be the correct procedure. This is due to it producing parameters as anticipated, a marked decrease in x dimensional cluster size and increase in the y which is as expected (figure 3,4). It also returns a multiplicity very close to the original unmapped data. Furthermore it shows that there is no appreciable difference between the two possible clustering

procedures, sparse and geometric, as they both return values that differ only at the fourth significant figure.

DAFFitter analysis was successful for both DESY sets, they both returned residuals which visually meet the expectations for the pixel pitches considered. The top hat functions in X are a result of the large pixel dimension; as such most hits will not be able to dissipate charge through multiple pixels in the X direction hence the vast majority of residuals will lie within ±250μm. The Gaussian shaped residual in the Y dimension similarly is explained through the smaller 25μm pixel pitch; this small size allows dissipation of charge across multiple pixels in the y axis resulting in more predicted hits having a residual larger than ±12.5μm. As expected the February 2014 data set indeed showed decreased performance in the irradiated detector through poorer residuals (figure 13, 14). It should be noted the RMS of the DAFFitter plots are larger than the anticipated uniform distribution calculated values. For a pixel pitch of 500μm one would expect a resolution of 144μm and for the partnering dimension of 25μm, an RMS of 7μm. GBL on the contrary produces resolutions almost matching this predicted magnitude (figure 9, 10, 11, 12).

For SLAC problems were encountered in using DAFFitter to fit the tracks. The extremely unresponsive hit map of the irradiated sensor (figure 29) and far away position of the reference detector likely contributed to this.
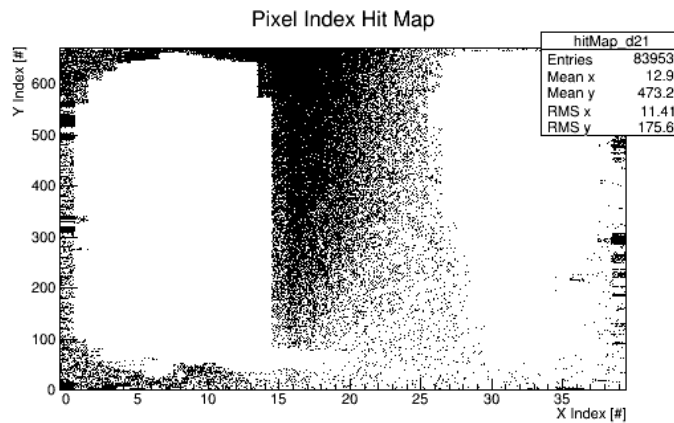

Figure 29: Irradiated Detector was stored for long periods of time and not sufficiently cooled. Could potentially have led to bump bonding problems

For GBL it was possible to fit with appropriate residuals for the irradiated sensor but with seemingly senseless output for the reference DUT. It was theorized that due to the reference DUT requiring a 180° ZX rotation to produce positive correlations that off sets introduced in alignment which were intended for a given axis were actually being propagated in the wrong direction due to the rotation of the local axis. This would cause a DUT shift farther away from its aligned position rather than closer and due to the high 12.5GeV occupancy of the SLAC data noisy hits near the edge of the detector were accidentally being matched as the closest hit to a track. This could then explain the extremely noisy residuals for this detector but upon investigating the linear algebra and source code, it was established that off sets should indeed be propagated in the correct direction regardless of the state of rotation. It is uncertain as to the cause of these residuals at this time.

Further investigation is warranted into the SLAC data to properly fit with both DAFFitter and GBL, discovering the reasons behind these anomalous plots should allow appropriate adjustments to be made to produce correct fits. Despite this the DESY data sets give insight into the comparison between DAFFitter and GBL. It shows that for not just both detectors but both data sets the residuals for GBL have an improved RMS over their DAFFitter counterparts and this is strong evidence suggesting that GBL is the superior approach to fitting.

5. Bibliography

[1] Comparing Geometries, K. Wraight, University of Glasgow, 2015.

[2] EUTelescope, 2015, Available at: http://eutelescope.web.cern.ch/ Accessed August 2015.

[3] Glasgow PPE twiki, 2015, Available at:
https://twiki.ppe.gla.ac.uk/bin/view/DetDev/EUTelescopeAndIBLTestbeam, Accessed August 2015.

[4] Havard Gjersdal, Test beam track reconstruction and analysis of ATLAS 3D pixel detectors, 2014

[5] Atlas Upgrade Project Introduction, K. Wraight, University of Glasgow, 2015